Phys. Status Solidi B **254,** No. 9, 1700089 (2017) / **DOI** 10.1002/pssb.201700089

physica status solidi b
www.pss-b.com
basic solid state physics

Electronic, elastic, lattice dynamic and thermal conductivity properties of Na_3OBr via first principles

Zhen-Long Lv*[,1], Hong-Ling Cui[1], Hui Wang[1], Xiao-Hong Li[1], and Guang-Fu Ji[2]

[1] School of Physics and Engineering, Henan University of Science and Technology, Luoyang 471023, P.R. China
[2] Institute of Fluid Physics, Chinese Academy of Engineering Physics, Mianyang 621900, P.R. China

Received 5 March 2017, revised 2 April 2017, accepted 18 April 2017
Published online 4 May 2017

Keywords electronic properties, first-principles calculation, ionic conductors, lattice dynamics, thermal conductivity

* Corresponding author: e-mail zhenlonglv@foxmail.com, Phone/Fax: +86 379 65626265

Na_3OBr is expected to be a promising superionic conductor for use as solid state electrolyte in large scale energy storage systems, but its lattice dynamic and thermal conductivity properties have not been well studied till now. In this work, we performed a detailed study on these properties as well as its electronic and elastic properties using first principles method. The results indicate that Na_3OBr is a direct band gap crystal. It is mechanically stable but elastically anisotropic. Its phonons at the Brillouin zone center were classified using group theory analysis and its Born effective charges, LO–TO splitting, and dielectric constants were calculated and discussed. Its phonon dispersion curves were obtained and their origins were revealed. Based on the phonon dispersion curves, its thermal conductivity as a function of temperature was predicted, which give a value of $7.30\,Wm^{-1}K^{-1}$ at 300 K. Further study reveals that, for Na_3OBr, the simple Slack's model can give almost the same thermal conductivity curve as that obtained from the phonon dispersion curves.

1 Introduction Perovskite-type compounds ABO_3 belong to cubic phase with the space group *Pm-3m*, where the eight vertexes are occupied by *A* cations, the body center is occupied by *B* cation, and the six face centers are occupied by oxygen anions. They have a lot of family members and are intensively studied due to their outstanding properties, such as ferroelectricity, exotic magnetism, superconductivity, and colossal magneto resistance [1]. Anti-perovskite compounds are similar to perovskites except that their face centers are occupied by metal cations instead of anions in normal perovskites. They are very interesting because they have many unique physical properties, such as almost zero temperature resistance coefficient [2] and negative thermal expansion [3], which make them promising materials for technological applications.

Some anti-perovskites such as Li-rich ones can be used as solid electrolyte for their non-flammable and non-toxic properties [4], high energy density, long-cycle lives [5], and superionic conductivity at moderate temperature [6]. Recently, researchers turn their eyes to Na-contained anti-perovskites because sodium is abundant in the earth's crust, which is expected to reduce the cost of ion batteries in large-scale energy storage systems [7], so they may find their use in electric vehicles and energy storing devices in the future. In addition, larger radius of Na ion is desirable for stabilizing the anti-perovskite structure as inferred from the tolerance factor of perovskites [8].

Na_3OBr, an anti-perovskite crystal, was reported to be one of the first alkali metal chalcogenide halides in 1988 [9]. It was only recently, when it was expected to be a competitive candidate for use in all-solid-state batteries, that it has become a hot object of study. In 2013, Ramanna et al. [10] studied its structural, elastic, electronic, and optical properties using two different density functional methods within generalized gradient approximation. In 2015, Wang et al. [11] tried to improve Na^+ conductivity in Na_3OBr by chemical manipulation techniques. In 2016, Zhu et al. [12] studied the transport mechanism of Na ions and found that they transport between the nearest Na ions in the NaO_6 octahedra. Nguyen et al. [7] experimentally investigated the effects of two processing approaches on the ionic conductivity of Na_3OBr and discovered a reduction in the activation energy. Wang et al. [13] studied its

structural stability under high pressure and found that it is stable under pressure up to 23 GPa.

However, there is still no first principles study on its lattice dynamic and thermal conductivity properties although it can further our understanding on the properties of this charming material and facilitate its application. Therefore, in this paper, we perform an in-depth and comprehensive study on the lattice dynamic and thermal conductivity properties as well as the electronic and elastic properties of Na_3OBr. The rest of this work are arranged as follows: the computational details are introduced in Section 2. In Section 3, the calculated electronic, elastic, lattice dynamic and thermal conductivity properties are presented and discussed. Finally, conclusions of this work are drawn in Section 4.

2 Computational details and methods

2.1 Computational details In this work, CASTEP [14] is used to perform the first principles calculations. Optimized norm-conserving pseudopotentials [15] are employed to evaluate the interaction between the electrons and nuclei, in which the electron configure for Na is $2s^2 2p^6 3s^1$, for O is $2s^2 2p^4$, and for Br is $4s^2 4p^5$. GGA-PBESOL [16] functional is chosen to calculate the exchange-correlation energy of electrons because it can give the most desirable relaxed lattice constants in the tests. Brillouin zone integration is processed using $4 \times 4 \times 4$ meshes based on the Monkhorst–Pack approach [17]. The wave functions are expanded by a chain of plane waves with a cutoff energy 800 eV. Tests show that these parameters ensure the energy converging to 5×10^{-6} eV/atom, the forces between ions converging to 0.01 eV Å^{-1} and the stress of the lattice to 0.02 GPa.

2.2 Elastic calculations Elastic constants reflect the mechanical behavior of a material within its elastic limit. The elastic constants C_{ijkl} ($i, j, k, l = 1$–6) of crystals can be computed using the definition [18]

$$C_{ijkl} = \left(\frac{\partial \sigma_{ij}(x)}{\partial e_{kl}}\right)_X, \quad (1)$$

where σ_{ij} is the applied stress, e_{kl} is the induced strain, X is the coordinate before the shape change of the crystal lattice, and x is the coordinate after the change.

For isotropic polycrystalline materials, it is hard to measure their individual elastic constant. In this case, aggregate qualities such as bulk modulus B, shear modulus G, Young's modulus E, and Poisson's ratio v are often used to denote their elastic performances. For a cubic crystal, its bulk modulus can be deduced using Voigt's and Reuss' approximations via [19]

$$B_V = B_G = (C_{11} + 2C_{12})/3. \quad (2)$$

Its shear modulus under these two approximations can be obtained respectively from the equations

$$G_V = (C_{11} - C_{12} + 3C_{44})/5, \quad (3)$$

$$G_R = [5C_{44}(C_{11} - C_{12})]/[4C_{44} + 3(C_{11} - C_{12})]. \quad (4)$$

Commonly used bulk and shear moduli are respectively their averages, i.e.,

$$B = (B_V + G_R)/2, \; G = (G_V + G_R)/2. \quad (5)$$

Young's modulus and Poisson's ratio can be derived from the expressions

$$E = 9BG/(3B + G), \; v = (3B - 2G)/2(3B + G). \quad (6)$$

Then, transverse V_t and longitudinal V_l sound velocities can be computed using the formulas [19]

$$V_t = [(3B + 4G)/\rho]^{1/2}, \; V_l = (G/\rho)^{1/2}. \quad (7)$$

Finally, Debye temperature θ_D can be assessed via

$$\Theta_D = \frac{h}{k}\left[\frac{3n}{4\pi}\left(\frac{N_A \rho}{M}\right)\right]^{1/3} V_m, \quad (8)$$

where h, k, and N_A are respectively the Plank constant, Boltzmann constant, and Avogadro constant, ρ is the density of the crystal, n is the number of atoms in the chemical formula, and M is the molecular mass. V_m is the average sound velocity, which can be obtained via the equation

$$V_m = \left[\left(2/V_t^3 + 1/V_l^3\right)/3\right]^{-1/3}. \quad (9)$$

3 Results and discussion

3.1 Structural relaxation Na_3OBr is a cubic anti-perovskite crystal with the space group *Pm-3m* (no. 221, point group O_h). Its lattice constant is $a = 4.5735$ Å [9] or 4.5674 Å [12] and the fractional coordination of Br is (0 0 0), of Na is (0 0 1/2), and of O is (1/2 1/2 1/2), see Fig. 1. To get

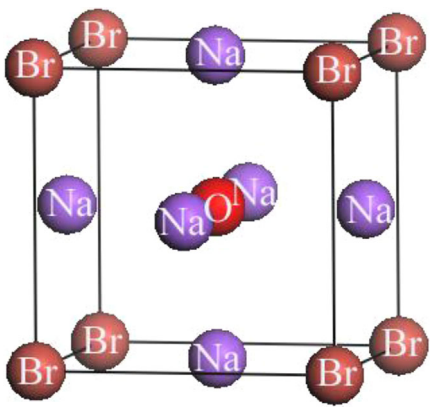

Figure 1 Crystal structure of Na_3OBr.

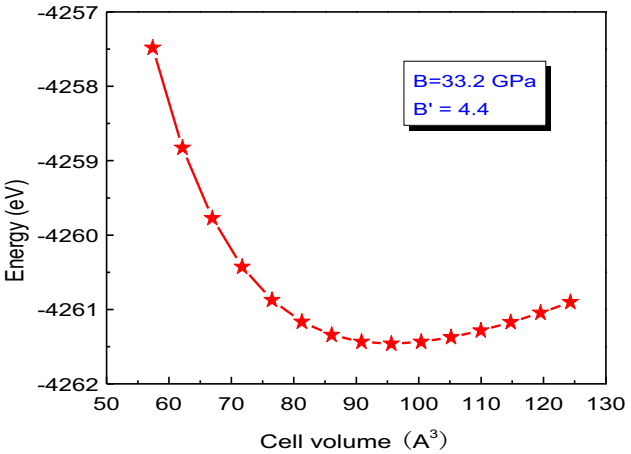

Figure 2 Fitted energy–volume curve of Na_3OBr.

the ground state of Na_3OBr, we changed the cell volume V and then calculated the corresponding energy E. The obtained E–V data are drawn in Fig. 2. By fitting them into the third-order Birch–Murnaghan equation of state (EOS) [20], we obtained a value 33.2 GPa as the bulk modulus of Na_3OBr and 4.4 as its first order pressure

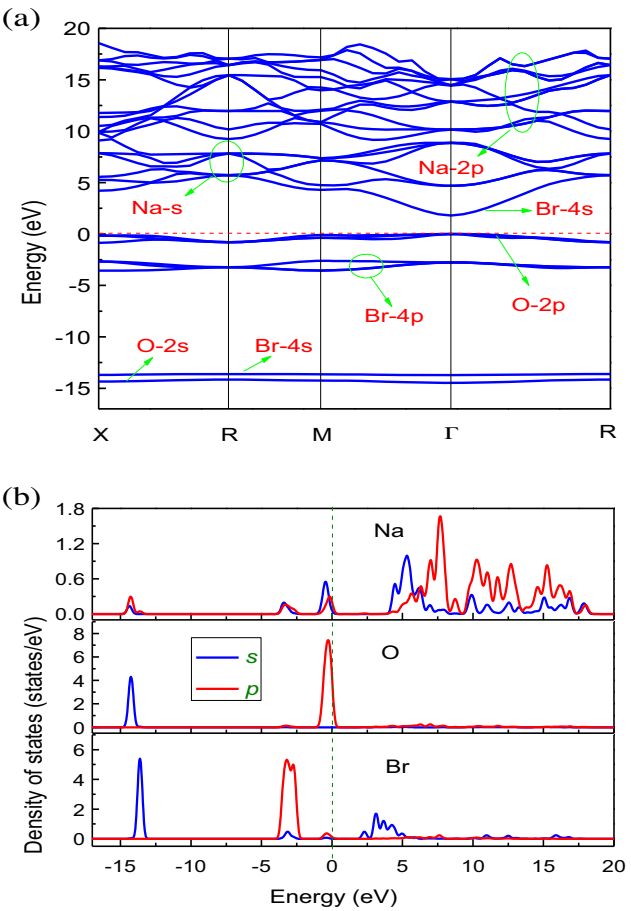

Figure 3 (a) Calculated electronic band structure and (b) partial density of states of Na_3OBr.

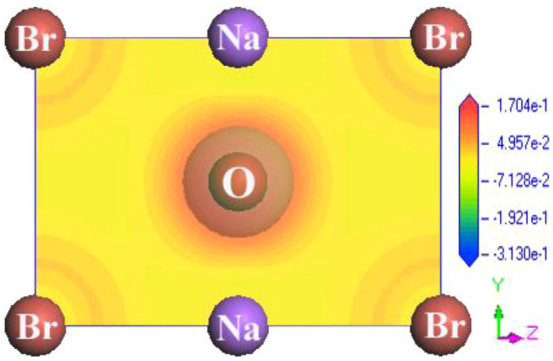

Figure 4 Electron density difference in the (110) plane of Na_3OBr, isosurface value: 0.1 e $Å^{-3}$.

derivative. The lattice constant a is deduced to be 4.5729 Å from the fitting, which has relative errors no more than 0.12% compared with the experimental values.

3.2 Electronic properties The calculated band structure along the high symmetry directions in the Brillouin zone is shown in Fig. 3(a). Both the covalence band maximum and the conduction band minimum are located at the Γ-point with a band gap of 1.81 eV, so Na_3OBr is a direct band gap insulator. It is seen that the bands below the Fermi level are rather flat, especially these at about −14 eV while these above the Fermi level seem much fluctuated. To find their origins, we calculated the partial density of states as shown in Fig. 3(b). The results uncover that the bands located at −14 eV originate from O-2s and Br-4s states, these at about −3 eV mainly come from Br-4p state, these just below the Fermi level are mainly from O-2p state, these in the energy range from 1.8 to 4 eV are formed by Br-4s state, and these above are contributed by Na-s and 2p. It is also seen that the hybridization among these states is very weak, so Na_3OBr is an ionic crystal. To verify this, we computed its electron density difference in the (110) plane as displayed in Fig. 4. It is illustrated that the electrons are around the O ion and no electrons accumulate between the cations and anions.

3.3 Elastic properties For cubic crystals, there are three independent elastic constants in their elastic tensors, i.e., C_{11}, C_{44}, and C_{66}. The calculated values for Na_3OBr are $C_{11} = 67.5$ GPa, $C_{44} = 20.9$ GPa, and $C_{12} = 14.7$ GPa, which agree, respectively, with the values 62.1, 19.8, and 15.8 GPa obtained by Ramanna et al. [10] using the FP-LAPW method and 70.0, 21.5, and 16.0 GPa reported by Deng et al. [21], but they are larger than the values 56, 17, and 13 GPa obtained by using force field method [22]. If a cubic crystal is mechanically stable, its elastic constants should satisfy the restrictions [19]: $C_{44} > 0$, $C_{11} - C_{12} > 0$, and $C_{11} + 2C_{12} > 0$. These of Na_3OBr meet above conditions, so it is mechanically stable. C_{12} is the smallest among these elastic constants, which means that when normal stress is exerted along one crystal axis, other two

vertical to it will have a larger strain. The large value of C_{11} results from the directional Na-O ionic bonds.

Bulk modulus mirrors the resistance of crystals against volume change and shear modulus measures its resistance against shape change. Bulk modulus of Na_3OBr deduced from elastic constants is 32.3 GPa, which coincides well with the value 33.2 GPa obtained by fitting the EOS above and the theoretical values 31.1 [10] and 34 GPa [21], but it is far smaller than the experimental value 58.6 GPa reported recently [13], the reason for which is still unknown. The shear modulus derived from elastic constants is 23.0 GPa, which is smaller than the bulk modulus, indicating that Na_3OBr is more vulnerable to shape deformation than volume change. The computed Young's modulus is 55.7 GPa, which is greater than the bulk modulus 32.3 GPa, meaning that Na_3OBr is more resistant against uniaxial tension or compression than hydrostatic pressure.

Pugh [23] suggested using the B/G ratio to distinguish the brittleness or ductility of materials. A value beyond 1.75 implies that it is ductile, if not, it is brittle. Calculated B/G ratio of Na_3OBr is 1.40, which means that Na_3OBr is brittle. Poisson's ratio is closely related to the bonding property of materials. A value of 0.25 signifies that the forces in that crystal are central [24]. This value of Na_3OBr is 0.21, which indicates that the interatomic forces in Na_3OBr are not perfect central. Debye temperature is an important parameter connecting with the thermal properties of solids. The predicted Debye temperature of Na_3OBr is 343.6 K, which is reasonable since it is lower than its synthetizing temperature 450 °C [7].

Solids are easy to crack if they have a large elastic anisotropy. Elastic anisotropy of a solid can be directly illustrated by its directional Young's modulus, which for cubic crystals is defined as follows [25]:

$$E = 1/[S_{11} - \beta(n_1^2 n_2^2 + n_1^2 n_3^2 + n_2^2 n_3^2)], \tag{10}$$

where $\beta = 2S_{11} - 2S_{12} - S_{44}$ and (n_1, n_2, n_3) are the direction cosines.

The computed directional Young's modulus and its (100) and (110) cross-sections of Na_3OBr are illustrated in Fig. 5. It is revealed that the maximum Young's modulus (62.2 GPa) is along the ⟨001⟩ directions while the minimum (51.6 GPa) is along the ⟨111⟩ directions, which indicates that ⟨001⟩ directions are stiffer than other directions, as reflected by the large value of C_{11}. If we define an anisotropy as: $A_E = 2(E_{max} - E_{min})/(E_{max} + E_{min})$, we will gain a value of about 18.6%, so Na_3OBr is a crystal of elastic anisotropy, which is the external expression of the non-central forces within Na_3OBr.

3.4 Phonons and dielectric properties

3.4.1 Phonons and LO–TO splitting The phonon frequencies at the Brillouin zone center (Γ-point) of a crystal can be deduced from its experimental infrared and Raman spectra. However, vibrational modes of phonons can be theoretically classified using the group theory analysis. There is one chemical formula in the primitive cell of Na_3OBr, so there are totally 15 phonon modes at the Γ-point, among which 3 are acoustic and 12 are optical. On the basis of group factor analysis, these optical modes can be divided into the following irreducible components:

$$\Gamma_{opt} = 3T_{1u}(I) + T_{2u}(S). \tag{11}$$

These optical modes include three threefold degenerated T_{1u} modes and one threefold degenerated T_{2u} mode, in which T_{1u} modes are infrared active and T_{2u} modes are silent. In order to give a further investigation, we calculated the vibrational frequencies and the corresponding eigenvectors of these modes. The results are listed in Table 1 and sketched in Fig. 6.

The calculated frequencies are all greater than those presented by Zinenko and Zamkova [22] due to that they used a classic force field method while we used the first principles method. From Fig. 6, we can see that the T_{2u} modes only involve the out of phase vibration of the two Na ions (Fig. 6(b)), which cannot induce dipole moment and deformation of the electronic cloud of this crystal, so they are silent. The T_{1u} modes with the lowest frequency 82.7 cm^{-1} (Fig. 6(a)) involve the motions of all the constituent ions: the Na and O ions vibrate in phase while

Table 1 Calculated vibrational frequencies (ω_{TO}/ω_{LO}) of the TO/LO phonons at the Γ-point of Na_3OBr, unit: cm^{-1}.

modes	T_{1u}			T_{2u}
ω_{TO}/ω_{LO}	82.7/114.0	206.7/229.8	370.8/427.8	107.2
cal. [22]	76.3/87.1	193.0/216.1	281.7/361.2	94.9

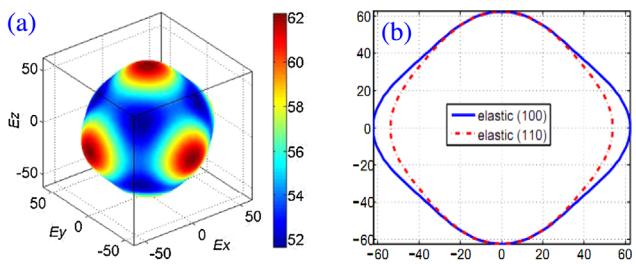

Figure 5 (a) Directional Young's modulus and (b) its (100) and (110) cross-sections of Na_3OBr.

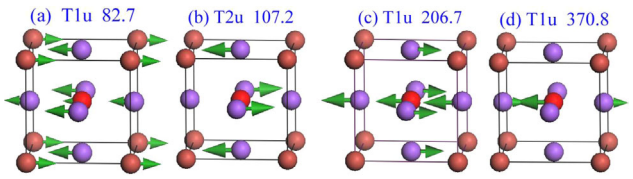

Figure 6 Vibrational frequencies (cm^{-1}) and their eigenvectors at the Γ-point of Na_3OBr.

Br ion vibrates oppositely. This kind of collective vibration will reduce the force constants between the ions, which results in a low vibrational frequency. In the T_{1u} modes with moderate frequency 206.7 cm^{-1} (Fig. 6(c)), O ion and one Na ion move in phase while other two Na ions vibrate oppositely. The T_{1u} modes with the highest frequency 370.8 cm^{-1} (Fig. 6(d)) originate from the out of phase vibrations of one Na ion and the O ion. This vibrational manner keeps a strong interaction between these ions and thus a high vibrational frequency.

3.4.2 Born effective charges In polar materials such as semiconductors and insulators, the long range characteristic of the Coulomb force between ions can produce a non-periodic electric field, which interacts with the longitudinal optical phonons leading to the splitting of the frequencies between them and the transverse phonons (LO–TO splitting) at the Γ-point. Born effective charge Z^* is such quantity measuring the strength of this kind of interaction and determining the amplitude of the LO–TO splitting [26]. The Born effective charge (BEC) $Z^*_{k,\beta\,\alpha}$ of ion k can be seen as the force F along α direction on ion k generated by an electric field E applied along β direction when ion k is constrained [27], i.e.,

$$Z^*_{k,\beta\alpha} = \frac{\partial F_{k,\alpha}}{\partial E_\beta}\bigg|_{\tau=0}. \tag{12}$$

Generally, the BECs of each constituent ion form a tensor (BECT), the form of which is decided by the symmetries of the crystal lattice and the ion position. For the high space symmetry of Na_3OBr, the BECs of its constituent ions are all diagonal, which indicate that moving the sublattice of Na, O, and Br along a given crystalline axis can only induce polarization in that direction. Na ions are located at the face centers, having a lower site symmetry, so they have two independent components $Z_{xx} = Z_{yy} = 1.09$, $Z_{zz} = 0.96$. O and Br ions are located at the center and vertex of the cubic lattice, therefore having one independent component −1.90 and −1.24, respectively. For a pure ionic crystal, the diagonal components of each constituent ion should be equal to its nominal ionic charge. The calculated BECs of Na, O, and Br are very close to their nominal ionic charges +1, −2, and −1, respectively, which confirms the ionic characteristic of Na_3OBr. Summing the BECs of all constituent ions in the cell finally gives a value of zero, which indicates that the polarization keeps invariant under rigid translation and meanwhile verifies the good convergence of our calculation.

3.4.3 LO–TO splitting and dielectric constants Since Na_3OBr is an insulator, we also calculated the frequencies of the longitudinal optical phonons and the results are included in Table 1. The amplitude of the splitting along a given direction can be decomposed into the contribution of each type of ion via [28]

$$\sum_m \left(\omega^2_{LO} - \omega^2_{TO}\right) = \frac{4\pi}{\varepsilon^\infty V}\sum_k \frac{(Z^*_k e)^2}{M_k}, \tag{13}$$

where m covers the infrared modes polarized along that direction, ε^∞ is the electronic dielectric constant, V is the cell volume, Z^*_k is the Born effective charge of ion k, and M_k is its mass.

Based on the above formula, we find that Na, O, and Br ions contribute 37, 58, and 5.0% to the LO–TO splitting, respectively. The large contribution of O stems from the fact that O has the largest Born effective charge −1.90 while the smallest atomic mass 16. For Na, although it has the smallest average Born effective charge of about 1.05, it has a smaller atomic mass 23 and a larger number, so its contribution is still considerable.

Dielectric constant mirrors the resistance of material against the applied electric field. In electric field with low frequency, both electrons and ions within crystals can be polarized, therefore they both contribute to the static dielectric constant. The electronic part can be calculated using DFPT method via the definition $\varepsilon^\infty_{\alpha\beta} = \delta_{\alpha\beta} + 4\pi \frac{\partial P_\alpha}{\partial E_\beta}|_{\tau=0}$, where α, β are the rectangular components and P is the macroscopic polarization along α direction caused by the exerted electric field E along β direction when the ions are bound. For cubic crystals, their electronic and ionic dielectric tensors are diagonal and only have one independent component. The calculated electronic dielectric constant of Na_3OBr is $\varepsilon^\infty_{\alpha\alpha} = 3.23$, which is larger than the reported theoretical value 2.20 [22]. This result gives a value 1.80 for its optical refractive index, but there is still no experimental value for us to compare with.

The static dielectric constant can be derived utilizing the formula [29]

$$\varepsilon_{\alpha\beta}(\omega) = \varepsilon^\infty_{\alpha\beta} + \frac{4\pi}{V}\sum_m \frac{S_{m,\alpha\beta}}{\omega^2_{TO,m}}, \tag{14}$$

$$S_{m,\alpha\beta} = \left[\sum_{k,\alpha'} Z^*_{k,\alpha\alpha'} U_m(k,\alpha')\right]\left[\sum_{k',\beta'} Z^*_{k',\beta\beta'} U_m(k',\beta)\right], \tag{15}$$

where ε^∞ is the electronic dielectric constant, m is the mth infrared mode, S_m is the oscillator strength of the mth infrared mode, $\omega_{TO,m}$ is the frequency of that mode, Z^*_k is the Born effective charge of ion k, and $U_m(k)$ is the normanized eigenvector. After calculating using the above formula, we gained the value $\varepsilon^0_{\alpha\alpha} = 10.09$ as the static dielectric constant of Na_3OBr, so the ionic contribution is 6.86, which is about two times as large as its electronic contribution.

3.5 Phonons and thermal conductivity To see the dynamic stability of Na_3OBr, we computed its phonon

dispersion curves and drew the results in the left panel of Fig. 7. No imaginary frequencies are found, which imply that Na_3OBr is dynamically stable. We also calculated its phonon partial density of states, as shown in the right panel of Fig. 7. It is revealed that the bands below 100 cm^{-1} are mainly aroused by the vibration of Br due to its large atomic mass, the bands above 350 cm^{-1} come principally from the vibration of O for its smaller atomic mass and Na ions contribute to the whole frequency range owing largely to the strong interaction between them and other two kind of anions. Figure 7 also reveals that the low-frequency optical modes couple with the acoustic ones, which will cause the heat-carrying acoustic modes to be scattered, thus affecting the thermal conductivity of Na_3OBr.

The thermal conductivity of an insulator is mostly controlled by its lattice vibration. Thermal conductivity of solids can be estimated using the semi-empirical formula [30]:

$$k_l(T) = \frac{0.849 \times 3\sqrt[3]{4}}{20\pi^3(1 - 0.514\gamma^{-1} + 0.228\gamma^{-2})} \times \left(\frac{k_B\Theta}{\hbar}\right)^2 \frac{k_B\overline{M}V^{1/3}}{\hbar\gamma^2}\frac{\Theta}{T}, \quad (16)$$

where $\overline{M}$, Θ, and γ are respectively the average atomic mass, the Debye temperature, and the Grüneisen parameter of that material. Here the latter two parameters are deduced from the phonon dispersion curves using the following expressions:

$$\Theta = n^{-1/3}\sqrt{\frac{5\hbar^2}{3k_B^2}\frac{\int_0^\infty \omega^2 g(\omega)d\omega}{\int_0^\infty g(\omega)d\omega}}, \quad (17)$$

$$\gamma^2 = \frac{\sum_i \int \frac{dq}{8\pi^3}\gamma_{iq}^2 C_{iq}}{\sum_i \int \frac{dq}{8\pi^3} C_{iq}}, \quad (18)$$

where n is the number of ions in the cell, ω is the frequency of phonon, $g(\omega)$ is the phonon density of states. γ_{iq} is the mode Grüneisen parameter and C_{iq} is its specific heat, both of which can be derived from the phonon frequencies via the definitions

$$\gamma_{iq} = -\frac{V}{\omega_{iq}}\frac{\partial\omega_{iq}}{\partial V}, \quad (19)$$

$$C_{iq} = k_B\left(\frac{\hbar\omega_{iq}}{k_BT}\right)^2 \frac{e^{-\hbar\omega_{iq}/k_BT}}{(e^{-\hbar\omega_{iq}/k_BT} - 1)^2}. \quad (20)$$

To our knowledge, the melting temperature of Na_3OBr is reported to be about 255 °C [11]. Another work indicates that Na_3OBr can be synthesized via solid-state reaction at about 450 °C [7]. To give a reasonable prediction, here we calculated its thermal conductivity at the temperatures from 200 to 800 K based on the above model. The results are displayed in Fig. 8 (starred curve).

It is shown that the thermal conductivity of Na_3OBr decreases when the temperature rises, which declines rapidly at low temperatures and then slowly. The reason is that the coupling between phonons weakens and the phonon mean-free path reduces to the average interatomic distance at high temperature [31]. At 300 K, the predicted thermal conductivity is about 7.30 $W\,m^{-1}\,K^{-1}$.

Thermal conductivity can also be simply estimated using Slack's model [32]: $k = A \cdot \frac{\overline{M}\Theta_D^3\delta}{(\gamma^2 n^{2/3}T)}$, where A is a constant ($A = 3.1 \times 10^{-6}$ if k is in $W\,m^{-1}\,K^{-1}$ and δ in Å), Θ_D is the Debye temperature obtained by Eq. (8), δ^3 is the volume per atom, γ is the Grüneisen parameter of the acoustic phonons at high temperature and can be deduced from Poisson's ratio through the expression $\gamma = \frac{3(1+\nu)}{[2(2-3\nu)]}$ [33] and other parameters are defined as these in Eq. (8). The obtained thermal conductivity of Na_3OBr as a function of temperature is also drawn in Fig. 8 (circled curve). It is seen that these two curves almost coincide with each other although the latter model is very simple, which

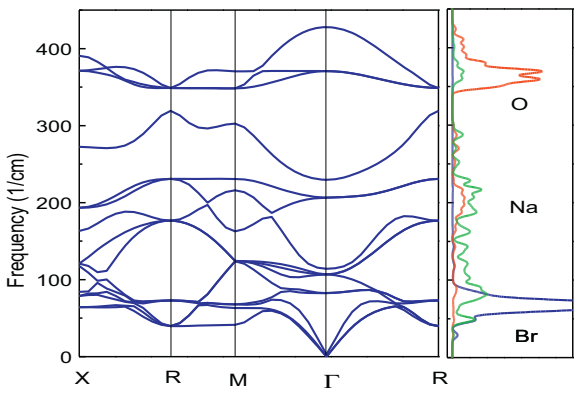

Figure 7 Phonon dispersion curves (left panel) and phonon partial density of states (right panel) of Na_3OBr.

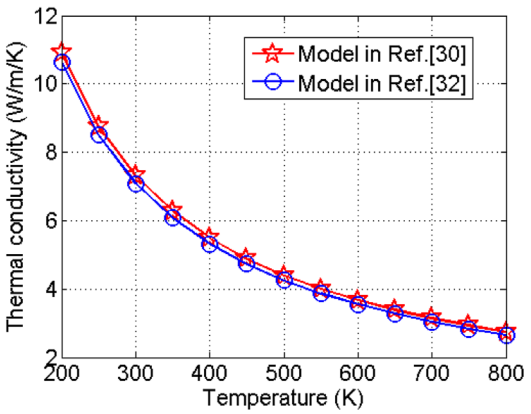

Figure 8 Calculated thermal conductivities of Na_3OBr.

may indicate that they have the same ability for predicting the thermal conductivity of cubic crystals although it is not completely true for other types [34].

Finally, it is worth to notice that, owing to the difference between these two computational methods, the Debye temperature calculated using Eq. (17) is only 230.4 K, which is considerably smaller than the value 343.6 K deduced from the elastic constants via Eq. (8). The Grüneisen parameter γ^2 derived from Eq. (18) is 2.66, which is remarkably larger than the value 1.80 deduced from Poisson's ratio. The same phenomenon also occurred in the case of SrClF [34].

4 Conclusions In summary, we studied the electronic, elastic, lattice dynamic and thermal conductivity properties of Na_3OBr by first principles method. Studies on its electronic properties reveal that Na_3OBr is an ionic crystal with a direct band gap of 1.81 eV. It has a bulk modulus of about 33 GPa and a shear modulus 23.0 GPa. Calculated directional Young's modulus indicates that Na_3OBr is elastically anisotropic, which may result from the non-central forces in it, as implied by its Poisson's ratio.

The three threefold degenerated T_{1u} modes are infrared active while the threefold degenerated T_{2u} modes are silent and the latter only involve the vibration of Na ions. Calculated Born effective charges of the constituent ions are close to their nominal chargers, which confirms the ionic characteristic of Na_3OBr. Investigations indicate that the LO–TO splitting is mainly contributed by O and Na and ions have about two times contribution to the total dielectric constant as the electrons.

Computed phonon dispersion curves indicate that Na_3OBr is dynamically stable. Two different methods were used to calculate the thermal conductivity of Na_3OBr. It is found that the thermal conductivity curve predicted by using the simple Slack's model nearly coincides with that obtained based on the phonon dispersion curves. At 300 K, the predicted thermal conductivity of Na_3OBr is about $7.30\ W\,m^{-1}\,K^{-1}$.

Acknowledgements This work is support by the National Natural Science Foundation of China under grant no. 11504089, the Key Scientific Research Projects of Henan Colleges and Universities under grant no. 17A140017 and the Innovation Team 2015XTD001 and Doctoral Scientific Research Foundation of Henan University of Science and Technology under grant no. 13480039.

References

[1] A. S. Bhalla, R. Guo, and R. Roy, Mater. Res. Innov. **4**, 3 (2000).
[2] E. O. Chi, W. S. Kim, and N. H. Hur, Solid State Commun. **120**, 307 (2001).
[3] P. Tong, D. Louca, G. King, A. Llobet, J. C. Lin, and Y. P. Sun, Appl. Phys. Lett. **102**, 041908 (2013).
[4] K. Xu, Chem. Rev. **104**, 4303 (2004).
[5] F. Cheng, J. Liang, Z. Tao, and J. Chen, Adv. Mater. **23**, 1695 (2011).
[6] Y. Zhao and L. L. Daemen, J. Am. Chem. Soc. **134**, 15042 (2012).
[7] H. Nguyen, S. Hy, E. Wu, Z. Deng, M. Samiee, T. Yersak, J. Luo, S. P. Ong, and Y. S. Meng, J. Electrochem. Soc. **163**, A2165 (2016).
[8] S. V. Krivovichev, Z. Kristallogr. **223**, 109 (2008).
[9] H. Sabrowsky, K. Paszkowski, D. Reddig, and P. Vogt, Z. Naturforsch. **43b**, 238 (1988).
[10] J. Ramanna, N. Yedukondalu, K. R. Babu, and G. Vaitheeswaran, Solid State Sci. **20**, 120 (2013).
[11] Y. Wang, Q. Wang, Z. Liu, Z. Zhou, S. Li, J. Zhu, R. Zou, Y. Wang, J. Lin, and Y. Zhao, J. Power Sources **293**, 735 (2015).
[12] J. Zhu, Y. Wang, S. Li, J. W. Howard, J. Neuefeind, Y. Ren, H. Wang, C. Liang, W. Yang, R. Zou, C. Jin, and Y. Zhao, Inorg. Chem. **55**, 5993 (2016).
[13] Y. Wang, T. Wen, C. Park, C. Kenney-Benson, M. Pravica, W. Yang, and Y. Zhao, J. Appl. Phys. **119**, 025901 (2016).
[14] M. D. Segall, P. L. D. Lindan, M. J. Probert, C. J. Pickard, P. J. Hasnip, S. J. Clark, and M. C. Payne, J. Phys.: Condens. Matter **14**, 2717 (2002).
[15] J. S. Lin, A. Qteish, M. C. Payne, and V. Heine, Phys. Rev. B **47**, 4174 (1993).
[16] J. P. Perdew, A. Ruzsinszky, G. B. I. Csonka, O. A. Vydrov, G. E. Scuseria, L. A. Constantin, X. Zhou, and K. Burke, Phys. Rev. Lett. **100**, 136406 (2008).
[17] H. J. Monkhorst and J. D. Pack, Phys. Rev. B **13**, 5188 (1976).
[18] D. C. Wallace, Thermodynamics of Crystals (Wiley, New York, 1972).
[19] X. L. Yuan, D. Q. Wei, Y. Cheng, G. F. Ji, Q. M. Zhang, and Z. Z. Gong, Comput. Mater. Sci. **58**, 125 (2012).
[20] F. Birch, J. Geophys. Res. **83**, 1257 (1978).
[21] Z. Deng, Z. Wang, I. H. Chu, J. Luo, and S. P. Ong, J. Electrochem. Soc. **163**, A67 (2016).
[22] V. I. Zinenko and N. G. Zamkova, Ferroelectrics **265**, 23 (2002).
[23] S. F. Pugh, Philos. Mag. **45**, 823 (1954).
[24] M. Mattesini, M. Magnuson, F. Tasnádi, C. Höglund, I. A. Abrikosov, and L. Hultman, Phys. Rev. B **79**, 125122 (2009).
[25] Z. L. Lv, H. L. Cui, H. Wang, X. H. Li, and G. F. Ji, Phys. Status Solidi B **253**, 1788 (2016).
[26] M. Veithen and P. Ghosez, Phys. Rev. B **65**, 214302 (2002).
[27] X. Gonze and C. Lee, Phys. Rev. B **55**, 10355 (1997).
[28] K. W. Lee and W. E. Pickett, Phys. Rev. B **68**, 085308 (2003).
[29] R. Eryiğit, C. Parlak, and R. Eryiğit, Eur. Phys. J. B **33**, 251 (2003).
[30] K. F. Garrity, Phys. Rev. B **94**, 045122 (2016).
[31] D. R. Clarke, Surf. Coat. Technol. **163–164**, 67 (2003).
[32] G. A. Slack, J. Phys. Chem. Solids **34**, 321 (1973).
[33] B. D. Sanditov, S. B. Tsydypov, and D. S. Sanditov, Acoust. Phys. **53**, 594 (2007).
[34] Z. L. Lv, H. L. Cui, H. Wang, X. H. Li, and G. F. Ji, Philos. Mag. **97**, 743 (2017).